Res Chem Intermed (2012) 38:1733–1742
DOI 10.1007/s11164-012-0498-9

Characterization and evaluation of the photocatalytic properties of wormhole-like mesoporous silica incorporating TiO_2, prepared using different hydrothermal and calcination temperatures

Babak Mazinani · Ali Beitollahi · Abdul Kadir Masrom · Noorhana Yahya · Thomas S. Y. Choong · Suhaina Mohd Ibrahim · Jafar Javadpour

Received: 28 November 2011 / Accepted: 19 January 2012 / Published online: 9 February 2012
© Springer Science+Business Media B.V. 2012

Abstract TiO_2–SiO_2 mesoporous materials were synthesised by deposition of TiO_2 nanoparticles prepared by the sol–gel method on to the internal pore surface of wormhole-like mesoporous silica. In this work we synthesised wormhole-like mesoporous silica of different surface area by changing the hydrothermal temperature (70, 100, or 130 °C). Subsequent to this, titania solution was deposited on to the inner surface of the pores and this was followed by calcination at different temperatures (400, 600, or 800 °C). The effect of different hydrothermal and calcination temperature on the photocatalytic properties was evaluated. The samples were characterized by N_2-sorption, X-ray diffraction, X-ray photoelectron spectroscopy, field emission scanning electron microscopy, and transmission electron microscopy. The effect of different hydrothermal and calcination temperatures on the photocatalytic properties was evaluated by measuring the degradation of

B. Mazinani (✉) · A. Beitollahi · J. Javadpour
Center of Excellence for Advanced Materials, School of Metallurgy and Materials Engineering, Iran University of Science and Technology (IUST), Narmak, Tehran, Iran
e-mail: b_mazinany@iust.ac.ir; b.mazinany@gmail.com

B. Mazinani · A. K. Masrom · S. M. Ibrahim
Industrial Nanotechnology Research Center, Lot 34, Jalan Hi-tech 2/3, Kulim Hi-Tech Park, 09000 Kulim, Kedah, Malaysia

N. Yahya
Faculty of Science and Information Technology, Universiti Teknologi Petronas, Tronoh, Perak, Malaysia

T. S. Y. Choong
Department of Chemical and Environmental Engineering, Faculty of Engineering, Universiti Putra Malaysia, 43400 UPM Serdang, Selangor, Malaysia

T. S. Y. Choong
INTROP, Universiti Putra Malaysia, 43400 UPM Serdang, Selangor, Malaysia

methylene blue in aqueous solution under UV light irradiation (mercury lamp, 125 W). The results indicated that appropriate surface area and degree of crystallinity are two important factors for obtaining high photocatalytic efficiency. Samples prepared at a hydrothermal temperature of 100 °C and calcined at 800 °C had the best photocatalytic performance, because of the highest surface area and high crystallinity.

Keywords Ceramics · Chemical synthesis · Chemical techniques · Surface properties

Introduction

TiO_2 has attracted much attention because of its excellent electronic and optical properties, for example photocatalysis, chemical sensing, and energy conversion [1]. It can be used for degradation of pollutants in aqueous solutions by using UV light irradiation [2]. The photocatalytic properties strongly depend on surface area, phase composition, and crystallinity. Because photocatalytic activity is a surface-based reaction, high surface area is always desirable [3]. Although reducing the size of TiO_2 particles will lead to increased surface area, filtering of small particles from solution is a problem in industrial usage [4, 5]. As an alternative, mesoporous TiO_2 has been studied as a candidate in order to achieve large particles with high surface area [6–8]. Problems in the synthesis of mesoporous titania, for example severe hydrolysis and condensation of Ti precursors [9–11], make it difficult to control the process and result in low thermal stability of the structure and phase transformation from anatase to rutile [12–15], which reduce photocatalytic efficiency [16, 17]; this has limited large-scale manufacture and application of this type of material. One alternative is to produce titanium dioxide supported on readily produced mesoporous silica. Use of a post-synthesis method is an important step, because blocking of pores can occur [18]. It has been well established that the photocatalytic properties of synthesised material can be greatly affected by pore size, surface area, and pore structure of the mesoporous silica [19–24]. SBA-15 [19–22], MCM41 [23], and MCF [24] have already been activated with TiO_2. Wormhole channel characteristics is a potentially important structural feature that leads to favourable catalytic activity, because channel branching within the framework can facilitate access to reactive sites on the framework walls [25].

Therefore, in this work, wormhole-like mesoporous silica was synthesised by use of hexane at different hydrothermal temperatures to investigate its effect on surface area. After removing the template by calcination, TiO_2 was deposited via the acid-catalysed sol–gel method. The prepared materials were then calcined at different temperatures. In particular, the effect of hydrothermal and calcination temperatures on photocatalytic performance and the structural properties of the materials were investigated.

Experimental

Materials

Pluronic triblock copolymer P123 poly(ethylene glycol)–poly(propylene glycol)–poly(ethylene glycol), $M_w = 5{,}800$, and titanium tetraisopropoxide (TTIP, 97%) were purchased from Aldrich. Tetraethoxysilane (TEOS, 98%) and HCl (37%) were obtained from Merck, and hexane (≥99%) was purchased from Baker.

Synthesis

Support

A typical synthesis was performed as follows. P123 (4 g) was dissolved in 30 g water and 120 g 2 M HCl solution and stirred for 5 h at 40 °C in a closed bottle. Hexane (molar ratio of hexane/P123 = 120) was pre-mixed with 9 g TEOS and then added to the solution with stirring. The mixture was then stirred for 24 h in a closed bottle and then transferred to a Teflon-lined autoclave for further reactions at different hydrothermal temperatures (70, 100, or 130 °C) for 48 h. All materials were filtered, washed with deionized water, and dried in a vacuum oven for 10 h. The solids were then calcined at 540 °C for 24 h to remove remaining surfactants. The synthesised materials were designated ST*x*, where *x* is hydrothermal temperature.

Post-modification

The procedure used for preparation of mesoporous TiO_2–SiO_2 samples followed the method described by Battacharyya et al. [26]. First, TTIP (weight ratio of SiO_2/TiO_2 = 2) was added to 30 mL 1 M HNO_3 solution with continuous stirring for 2.5 h. The colloidal solution was diluted with 50 mL of water and the pH was adjusted to 3 with 1 M NaOH. At pH 3 there is an electrostatic interaction between the positively charged TiO_2 and the negatively charged SiO_2 material. Subsequently, 0.5 g mesoporous silica was added and the mixture was stirred for 2 h. The resulting material was isolated by filtration, washed, dried, and finally heated at different temperature (400, 600, and 800 °C) for 3 h, with a heating rate of 5 °/min. The prepared materials are designated ST*x*−*y*, where *x* and *y* are, respectively, the hydrothermal temperature of the supporting material and the calcination temperature of post-modified materials.

Characterization

The surface area of all prepared samples were characterized and measured by nitrogen adsorption–desorption (BET) using the Autosorb-1 from Quantachrome Instruments. Before surface area measurement, samples were degassed at 250 °C for 6 h. Structural characterization of the materials was performed by X-ray diffraction (XRD). The XRD patterns were recorded with a Bruker powder X-ray

diffractometer using a Cu radiation source of wavelength 1.54 Å ranging from 20° to 80° with a scan speed of 0.04 °/s at 40 kV and 40 mA. The morphology of the samples was characterized by scanning electron microscopy (SEM, LEO-1525) with an accelerating voltage of 20 kV. X-ray photoelectron spectroscopy (XPS) spectra was recorded by use of an Omicron Nanotechnology (ELS5000) system using Al kα radiation at a base pressure below 5.5×10^{-9} Torr. Transmission electron microscopy (TEM) was performed with a Philips Tecnai 20 microscope operated at 200 kV.

Photocatalytic activity measurement

The photocatalytic activity of the sample was evaluated by measuring the degradation of methylene blue (MB; Sigma–Aldrich, >97%) in aqueous solution under UV light irradiation (mercury lamp, 125 W). In a typical experiment, 30 mg TiO_2 was dispersed in 100 mL MB solution of concentration 40 mg/L. The amount of mesoporous material used was the amount necessary to achieve the same TiO_2 loading as for the commercial nanoporous photocatalyst P25. The mixture was first stirred for 30 min in the dark. The concentration of MB in the mixture was determined by UV–visible spectrometry (Lambda 25 Perkin–Elmer) after centrifuging.

Results and discussion

Structural and photocatalytic properties of samples calcined at 400 °C

In this work, at first wormhole-like mesoporous silica was synthesised successfully and then the TiO_2–SiO_2 materials were prepared. TEM and SEM patterns of the ST100-400 sample are shown in Fig. 1a and b respectively. In addition, EDX maps are presented in Fig. 1c, d. It is clear that the Si and Ti in the particles are homogeneously distributed.

Nitrogen adsorption–desorption isotherms of the samples synthesized at different hydrothermal temperatures (70, 100, or 130 °C), before and after introduction of TiO_2, are presented in Fig. 2a and b, respectively.

As can be seen in Fig. 2a, although the hysteresis loops of all samples are type IV isotherms, the shapes of the loops vary substantially with different hydrothermal temperature. For low hydrothermal temperature, a broad loop was obtained, because of the presence of narrow passages inside the pores [27–29]. For higher hydrothermal temperatures, the hysteresis loops are narrower. The insets show the pore size distribution calculated by use of the BJH method. Analysis revealed that increasing the hydrothermal temperature increased the mean pore size. A broad pore-size distribution was achieved for sample prepared at a hydrothermal temperature of 130 °C (ST130), which could be because of a higher vapour pressure of hexane inside the pores during the hydrothermal process [27, 28]. On the other hand, although the shape of the loops before and after impregnation is similar (Fig. 2a, b), the pore volume and surface area are substantially affected (Table 1).

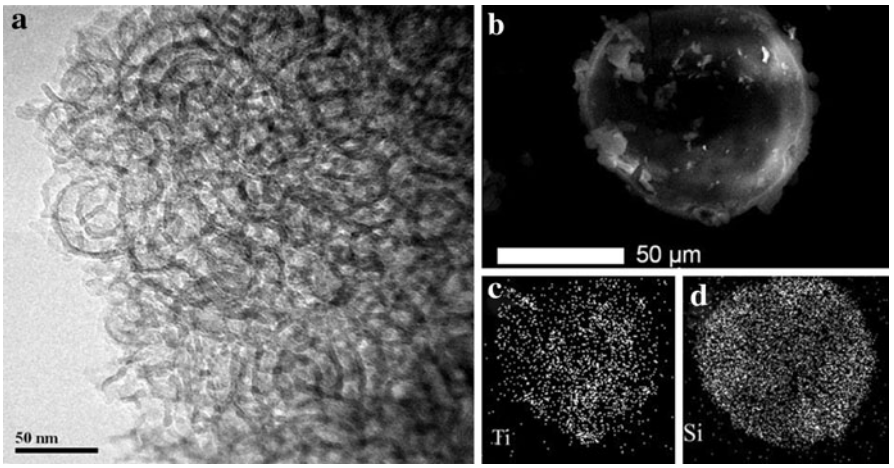

Fig. 1 TEM micrograph (**a**), SEM micrograph (**b**), and EDX maps of silicon and titanium of the ST100-400 sample (**c**, **d**)

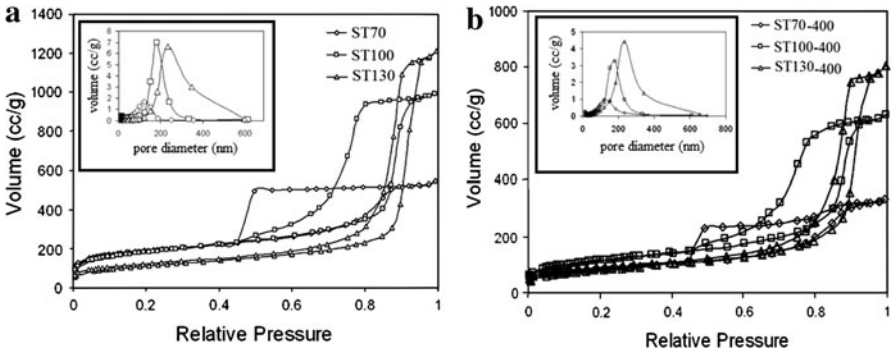

Fig. 2 N_2 isotherms with pore size distribution calculated by use of the BJH method **a** before and **b** after introducing TiO_2 to mesoporous silica prepared at different hydrothermal temperatures

Table 1 Textural properties of the samples

Sample ID	S_{BET} (m^2/g)[a]	D (nm)[b]	V (cm^3/g)[c]
ST70	706	5.3	0.9
ST100	629	9.8	1.5
ST130	396	19	1.9
ST70-400	408	7.2	0.7
ST100-400	395	9.8	1
ST130-400	283	17.6	1.2
ST70-800	190	9	0.4
ST100-800	324	10.8	0.9
ST130-800	251	18.9	1.2

[a] BET surface area

[b] Mean BJH pore diameter

[c] Adsorption total pore volume

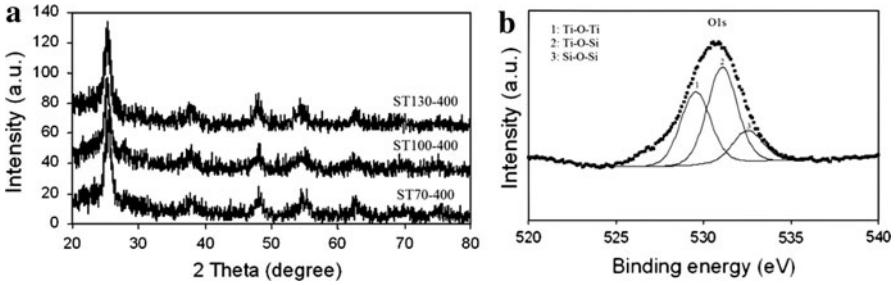

Fig. 3 **a** XRD patterns of samples calcined at 400 °C, and **b** XPS spectra of the ST70-400

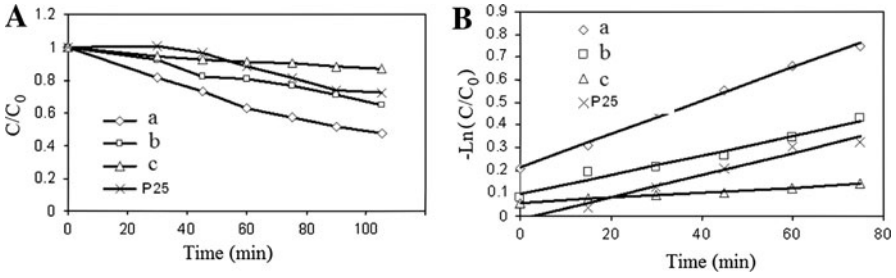

Fig. 4 **A** photodegradation of MB by UV light, and **B** photodegradation kinetic curve in the presence of (*a*) ST70-400, (*b*) ST100-400, (*c*) ST130-400, and Degussa P25

These results indicate that TiO_2 particles have been dispersed in the pores of mesoporous materials, leading to a reduction in pore volume and surface area [21].

The XRD patterns of samples calcined at 400 °C are shown in Fig. 3a. The patterns show that anatase is the only TiO_2 crystalline phase. For all samples calcined at 400 °C, the crystallite size was estimated, by use of the Scherrer formula, to be approximately 12 nm.

To understand the surface structure of the photocatalysts, the XPS technique was used. The O(1s) XPS peak for ST70-400 is best fitted with three component peaks (Fig. 3b). The peaks at 532.6 and 529.6 eV are assigned to oxygen in Si–O–Si and Ti–O–Ti bonds, respectively. In addition, a peak at an intermediate binding energy (531.1 eV) was assigned to oxygen in Si–O–Ti [30].

Photocatalytic performance was investigated by degradation of MB in aqueous solution under UV light irradiation. Figure 4A shows the photocatalytic results for samples calcined at 400 °C. For comparison, the photocatalytic activity of commercial nanoporous photocatalyst P25 was also measured under the same conditions.

It is well known that the rate of photodegradation can be described by use of pseudo-first-order kinetics, and the rate constant for degradation, k, can be estimated as follows:

$$-\ln\left(\frac{C}{C_0}\right) = kt \tag{1}$$

where C_0 is the initial absorbance of the MB dye and C is the absorbance after time t [31]. The related graphs are presented in Fig. 4B.

Elimination of MB can be caused by adsorption on the surface of the photocatalyst or by photodegradation. To evaluate the photodegradation of MB, the suspension was initially stirred for 30 min in the dark to reach the adsorption–desorption equilibrium.

The efficiency of titania can be related to the phase composition (rutile or anatase), surface area, crystallinity, electron–hole recombination, number of electrons created, and the size of TiO_2 nanoparticles [32]. As can be seen in Fig. 4, ST70-400 (hydrothermal temperature 70 °C) with the highest surface area (408 m^2/g) resulted in the highest rate of photodegradation ($k = 0.0073$ min^{-1}) whereas ST130-400 (hydrothermal temperature 130 °C) with the lowest surface area (283 m^2/g) resulted in the lowest rate of photodegradation ($k = 0.0011$ min^{-1}).

Effects of calcination temperature

Figure 5a and b show the WAXRD patterns of the samples calcined at 600 and 800 °C, respectively. The results indicate that anatase is the only phase present in all the samples. It is well known that the presence of TiO_2 and the SiO_2 mesostructure can retard the phase transformation from anatase to rutile during calcination and improve the photocatalytic properties [21]. As the temperature increased, the peaks of the anatase phase became stronger and sharper. Estimation by use of Scherer's equation revealed the average crystallite size for samples calcined at 600 and 800 °C was approximately 14 and 17 nm, respectively.

Because of growth of TiO_2 particles inside the pores with increasing calcination temperature, the physical properties of the pores can be affected. N_2 adsorption–desorption isotherms and pore size distribution of samples calcined at 800 °C are presented in Fig. 6, and their structural characteristics are summarised in Table 1.

For ST70-800, surface area decreases dramatically. This can be attributed to plugging of small pores by growing TiO_2 particles with increasing calcination temperature.

The photocatalytic properties of samples calcined at 600 and 800 °C are presented in Fig. 7A and B, respectively. It can be seen that all of the samples result in better elimination of MB than P25 titania. To assess the effect of calcination

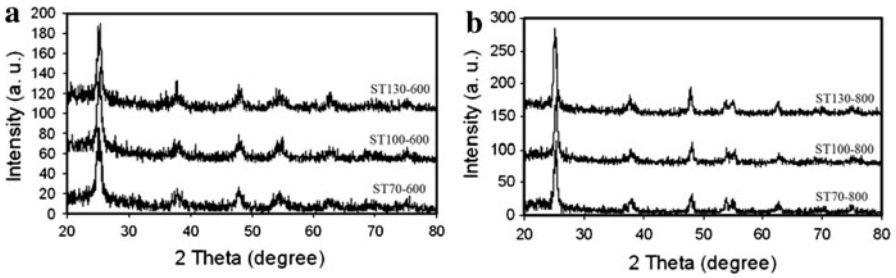

Fig. 5 WAXRD of samples calcined at **a** 600 °C and **b** 800 °C

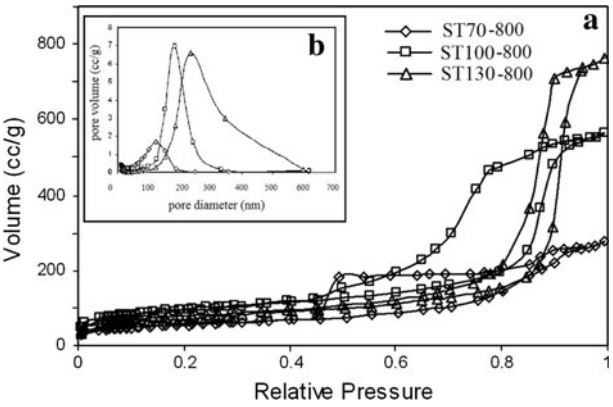

Fig. 6 N_2 adsorption–desorption isotherm and pore size distribution (*inset*) of samples calcined at 800 °C

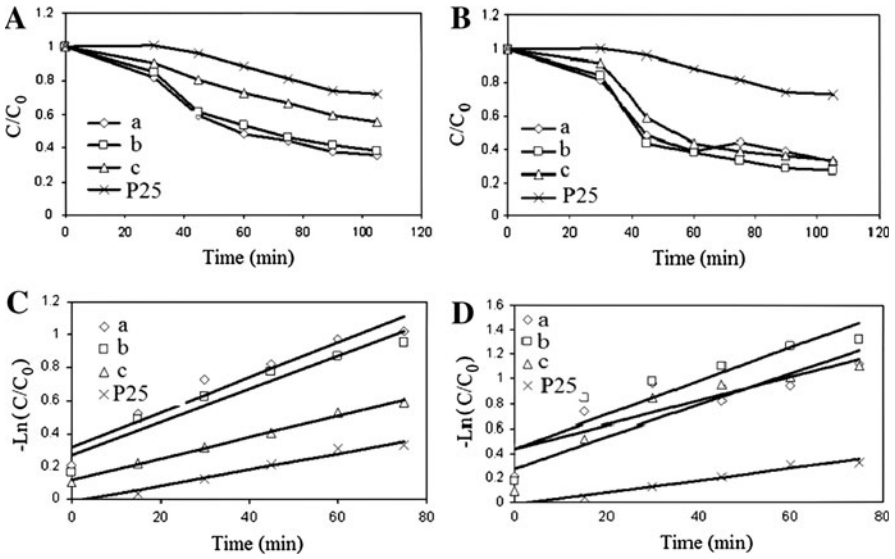

Fig. 7 **A** and **B** UV light photodegradation effect on MB. **C** and **D** Photodegradation kinetic curve in the presence of (*a*) ST70-400, (*b*) ST100-400, and (*c*) ST130-400 calcined at 600 °C (**A** and **C**) and 800 °C (**B** and **D**)

temperature on photocatalytic efficiency, the photodegradation kinetic curves were determined for samples calcined at 600 and 800 °C; the plots are shown in Fig. 7C and D, respectively.

The rate constants for all the samples are depicted in Fig. 8.

Two important factors that significantly affect the photocatalytic activity of mesoporous SiO_2–TiO_2 are surface area and the degree of crystallinity. It has been well established that photocatalysis is a surface-based reaction, therefore a higher

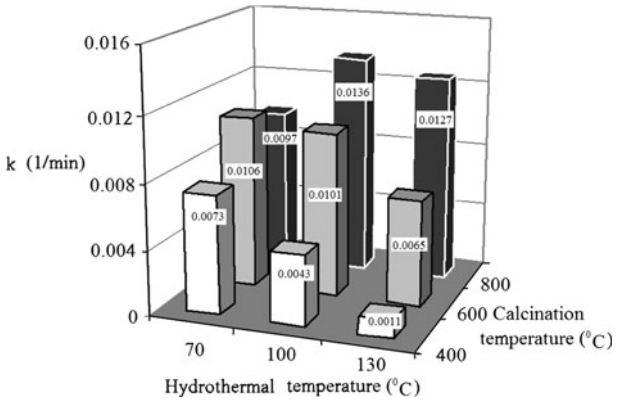

Fig. 8 Effect of hydrothermal temperature and calcination temperature on photocatalytic rate constant

surface area improves photocatalytic efficiency because of the availability of more reaction sites [3].

As shown in Fig. 8, for samples that were calcined at 400 °C, ST70-400 has the highest photocatalytic activity because of its high surface area (408 m^2/g). Increasing the calcination temperature from 400 to 600 °C, improves the photocatalytic efficiency (Fig. 8) because a higher calcination temperature increases crystallinity. Interestingly, for samples prepared at a hydrothermal temperature of 70 °C, a further increase in calcination temperature (600–800 °C) results in a decrease in photocatalytic performance because of a decrease in surface area (190 m^2/g). This phenomenon can be related to collapsing of pores as TiO_2 particles grow at higher temperatures. In other words, although a higher calcination temperature results in greater crystallinity, which should improve photocatalytic performance, it can also lead to a drastic decrease of surface area, which results in reduced photocatalytic performance. For samples prepared at hydrothermal temperatures of 100 and 130 °C, photocatalytic activity improved with increasing calcination temperature from 600 to 800 °C. The photocatalytic performance of ST100-800 was better than that of ST130-800 because of greater surface area (Table 1).

Conclusion

It was established that surface area and crystallinity are the two main factors that significantly affect the photocatalytic activity of mesoporous TiO_2–SiO_2 photocatalyst. Results showed that a wormhole-like structure is suitable for degradation of MB, and the photocatalytic activity of all the calcined powder samples was higher than that of Degussa P25 except for the sample prepared at the highest hydrothermal temperature (130 °C) and calcined at the lowest temperature (400 °C). The best photodegradation of MB was obtained by use of the sample which was treated hydrothermally at 100 °C and calcined at 800 °C, because of the relatively high surface area and a high degree of crystallinity.

Acknowledgments Mr Mohamad Hazri, Ms Zuhana Ahmad Zuber, and Dr Mat Husin Saleh are gratefully acknowledged for their assistance during the BET and TEM experiments. This work was supported by the SIRIM bhd and Iran University of Science and Technology (IUST) through a collaborative research program. The authors are also grateful to Universiti Putra Malaysia and Universiti Teknologi Petronas for their kind assistance in performing some of the characterization work.

References

1. R. Asahi, T. Morikawa, T. Ohwaki, K. Aoki, Y. Taga, Science **293**, 269 (2001)
2. G. Li, Z. Zhao, J. Liu, G. Jiang, J. Hazard. Mater. **192**, 227 (2011)
3. X. Fan, T. Yu, L. Zhang, X. Chen, Z. Zou, Chin. J. Chem. Phys. **20**, 733 (2007)
4. N. Xu, Z. Shi, Y. Fan, J. Dong, J. Shi, M.Z.-C. Hu, Ind. Eng. Chem. Res. **38**, 373 (1999)
5. B. Ohtani, Y. Ogawa, S.-I. Nishimoto, J. Phys. Chem. B **101**, 3746 (1997)
6. E.-Y. Kim, D.S. Kim, B.T. Ahn, Bull. Korean Chem. Soc. **30**, 193 (2009)
7. J. Wang, Y. Zhou, Y. Hu, R. O'Hayre, Z. Shao, J. Phys. Chem. **115**, 2529 (2011)
8. D. Chen, F. Huang, Y.-B. Cheng, R.A. Caruso, Adv. Mater. **21**, 2206 (2009)
9. G.J. de A.A. Soler-Illia, C. Sanchez, B. Lebeau, J. Patarin, Chem. Rev. **102**, 4093 (2002)
10. P. Yang, D. Zhao, D.I. Margolese, B.F. Chmelka, G.D. Stucky, Nature **396**, 152 (1998)
11. G.J. de A.A. Soler-Illia, A. Louis, C. Sanchez, Chem. Mater. **14**, 750 (2002)
12. B. Tian, H. Yang, X. Liu, S. Xie, C. Yu, J. Fan, B. Tu, D. Zhao, Chem. Commun. 1824 (2002)
13. M.D. Perez, E. Otal, S.A. Bilmes, G.J.de A.A. Soler-Illia, E.L. Crepaldi, D. Grosso, C. Sanchez, Langmuir **20**, 6879 (2004)
14. S.Y. Choi, B. Lee, D.B. Carew, M. Mamak, F.C. Peiris, S. Speakman, N. Chopra, G.A. Ozin, Adv. Funct. Mater. **16**, 1731 (2006)
15. H.X. Li, Z.F. Bian, J. Zhu, Y.N. Huo, H. Li, Y.F. Lu, J. Am. Chem. Soc. **129**, 4538 (2007)
16. X. Ding, X. Liu, J. Mater. Res. **139**, 2556 (1998)
17. J. Ovenstone, K. Yanagisawa, Chem. Mater. **11**, 2770 (1999)
18. Y.C. Lee, S. Cheng, J. Chin. Chem. Soc. **53**, 1355 (2006)
19. H. Ding, H. Sun, Y. Shan, J. Photochem. Photobiol. A **169**, 101 (2005)
20. W. Wang, M. Song, Microporous Mesoporous Mater. **96**, 255 (2006)
21. J. Yang, J. Zhang, L. Zhu, S. Chen, Y. Zhang, Y. Tang, Y. Zhu, Y. Li, J. Hazard. Mater. **137**, 952 (2006)
22. W. Wang, M. Song, Mater. Res. Bull. **41**, 436 (2006)
23. R. Van Grieken, J. Aguado, M.J. López-Muños, J. Marugán, J. Photochem. Photobiol. A **148**, 315 (2002)
24. E. Beyers, E. Biermans, S. Ribbens, K. De Witte, M. Mertens, V. Meynen, S. Bals, G. Van Tendeloo, E.F. Vansant, P. Cool, Appl. Catal. B **88**, 515 (2009)
25. T.R. Pauly, Y. Liu, T.J. Pinnavaia, S.J.L. Billinge, T.P. Rieker, J. Am. Chem. Soc. **121**, 8835 (1999)
26. A. Battacharyya, S. Kawi, M.B. Ray, Catal. Today **98**, 431 (2004)
27. K. Kruk, L. Cao, Langmuir **23**, 7247 (2007)
28. J. Sun, H. Zhang, D. Ma, Y. Chen, X. Bao, A. Klein-Hoffmann, N. Pfander, D.S. Su, Chem. Commun. 5343 (2005)
29. P. Van Der Voort, M. Benjelloun, E.F. Vansant, J. Phys. Chem. B **106**, 9027 (2002)
30. Z.L. Hua, J.L. Shi, L.X. Zhang, M.L. Ruan, J.N. Yan, Adv. Mater. **14**, 830 (2002)
31. Y.Z. Li, S.J. Kim, J. Phys. Chem. B **109**, 12309 (2005)
32. Q.Z. Yan, T.S. Xin, Z.Y. Huang, C. Ge, J. Eur. Ceram. Soc. **26**, 915 (2006)